

TSSD: Temporal Single-Shot Object Detection Based on Attention-Aware LSTM

Xingyu Chen^{1,2}, Zhengxing Wu¹, Junzhi Yu¹

¹ Institute of Automation, Chinese Academy of Sciences, Beijing, China.

² University of Chinese Academy of Sciences, Beijing, China

{chenxingyu2015, zhengxing.wu, junzhi.yu}@ia.ac.cn

Abstract

Temporal object detection has attracted significant attention, but most popular detection methods can not leverage the rich temporal information in video or robotic vision. Although many different algorithms have been developed for video detection task, real-time online approaches are frequently deficient. In this paper, based on attention mechanism and convolutional long short-term memory (ConvLSTM), we propose a temporal single-shot detector (TSSD) for robotic vision. Distinct from previous methods, we take aim at temporally integrating pyramidal feature hierarchy using ConvLSTM, and design a novel structure including a high-level temporal unit as well as a low-level one (HL-TU) for multi-scale feature maps. Moreover, we develop a creative temporal analysis unit, namely, attention-aware ConvLSTM (AC-LSTM), in which a temporal attention module is specially tailored for background suppression and scale suppression while ConvLSTM temporally integrates attention-aware features. An association loss is designed for temporal coherence. Finally, our method is evaluated on ImageNet VID dataset. Extensive comparisons on the detection capability confirm or validate the superiority of the proposed approach. Consequently, the developed TSSD is fairly faster and achieves an overall competitive performance in terms of mean average precision. As a temporal, real-time, and online detector, TSSD is applicable to robot's intelligent perception.

1. Introduction

With the rapid development of computer vision, the robot is competent in visually perceiving environments gradually. For example, Nguyen *et al.* designed an affordances detection method to help a robot plan grasp [1]; On the other hand, Object detection is one of the important vision tasks, which has developed for years. However, recent works have largely focused on detecting in static images, so they are not suited to temporally concordant robotic vision. Thus, it is essential to develop an approach to integrate

spatial features with temporal information for robot's intelligent perception.

Taking advantage of the convolutional neural network (CNN), existing detection methods can be divided into two categories, i.e., one-stage and two-stage detectors. The former is represented by RCNN family [2, 3, 4, 5], RFCN [6], and FPN [7], all of which detect objects based on region proposal. On the other hand, YOLO [8], SSD [9], and RetinaNet [10] treat the localization task as a regression, and the regression and classification can be computed simultaneously with single-shot multi-box algorithms. In particular, making use of CNN's features more effectively, SSD is one of the first methods that adopt the pyramidal feature hierarchy for detection. Considering the two-stage detectors have better detection precision and their region proposal can be generalized to process consecutive frames, researchers tend to apply two-stage detection methods to video detection sphere. However, the one-stage detectors have an advantage of faster inference speed. Therefore, the temporal performance of one-stage detector deserves to be studied take for both the precision and inference speed.

Recurrent neural network (RNN) has achieved great success in some sequence processing tasks [11, 12]. Typically, long short-term memory (LSTM) is proposed for longer sequence learning [13]. For spatiotemporal visual features, Shi *et al.* developed convolutional LSTM (ConvLSTM) to associate LSTM with spatial structure [14]. However, the total amount of CNN's feature for detection is very huge, especially when pyramidal features are adopted, so a temporal model for multi-scale feature maps should be built. Moreover, only a small part of visual features devote themselves to detecting targets, since background takes up most of the image. Therefore, if the whole features are fed to it, ConvLSTM will be confused by vast useless information. Thus, the feature selection is a pivotal step. Fortunately, attention is an exciting idea which imitates human's cognitive patterns, promoting CNN concern something essential. For example, Mnih *et al.* proposed a recurrent attention model (RAM) to find the most suitable local feature for image classification [16]. However, attention model for

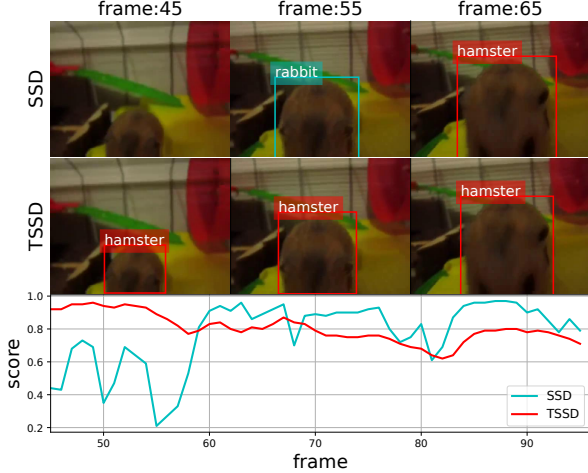


Figure 1. Example results. This is a changing validation video snippet containing a hamster. With large temporal fluctuations in terms of detection score, SSD’s results contain the false positive and false negative, whereas the performance of TSSD is more stable and accurate.

image-sequence detection is still deficient. According to aforementioned knowledge, an model is able to extract key information in an image sequence, helping ConvLSTM escape from vast information redundancy. In turn, ConvLSTM is capable of modeling spatiotemporal feature for detection and helping attention model perceive what should be focused more accurately.

In this paper, taking aim at detecting objects in robotic vision, we propose a temporal detection model based on SSD, namely, temporal single-shot detector (TSSD), whose example results are illustrated in Fig. 1. To integrate features through time, ConvLSTM is employed for temporal information. Due to the pyramidal feature hierarchy for multi-scale detection, SSD always generates a large body of visual features for static regression and classification, so a ConvLSTM is hard to integrate these multi-scale feature maps. Then, if ConvLSTMs are utilized for each feature map, the dramatically increasing parameters could reduce inference speed. Thus, we design a new structure including a high-level temporal unit as well as a low-level one (HL-TU) for multi-scale features. Furthermore, as for a image, only a small part of visual features are related to objects. Thereby, we propose a creative module to integrate spatiotemporal information, namely, attention-aware ConvLSTM (AC-LSTM), in which overfull useless information is prevented from being fed to ConvLSTM. That is, a temporal attention module selects essential features for a ConvLSTM. Further, the ConvLSTM integrates spatiotemporal features for detection and simultaneously helps the attention module find better focus points in turn. Subsequently, an association objective is developed for sequence training. Fi-

nally, facilitated by above-mentioned improvements, TSSD achieves considerable detection performance for consecutive vision in terms of both precision and speed. To the best of our knowledge, only few temporal one-stage detectors has been reported, and few temporal structures have been designed for pyramidal visual features.

The contributions made in this paper are summarized as follows: i) To temporally integrate pyramidal feature hierarchy, we design a HL-TU structure to effectively propagate multi-scale visual features through time. ii) We propose an AC-LSTM framework as a temporal analysis unit, in which redundant information is reduced. As a result, ConvLSTM can attentively process objects’ features. iii) An association loss function is developed for temporal coherence. iv) We achieve a considerably improved result on ImageNet VID dataset, i.e., a mAP of 65.43%, and an average inference speed of 27 FPS.

2. Related Work

2.1. Post-Processing Method

At the beginning, static detection and post-proposing methods are combined to counteract video detection task [17, 18, 19]. They statically detect in each video frame, and then, comprehensively deal with multi-frame results. Kang *et al.* developed detection methods based on tubelet, which is defined as temporally propagative bounding boxes in video snippet [17, 18]. Their method TCNN contains still-image object detection, multi-context suppression (MCS), motion guided propagation (MGP), and temporal tubelet re-scoring. MCS and MGP reduce false positives and false negatives with context and motion information. For long-term memory, temporal tubelet re-scoring generates tubelets by tracking. Taking inspire from non-maximum suppression, Han *et al.* proposed SeqNMS to suppress temporally discontinuous bounding boxes. However, due to complex post-processing, the time efficiency decreases. Moreover, such methods do not improve the performance of the detector itself.

2.2. Detection Based on Region Proposal

Faster RCNN uses region proposal network for object localization [4], so some approaches for video detection try to enhance the effectiveness of RPN with temporal information [20, 21, 22, 28, 40]. Galteri *et al.* designed a closed-loop RPN, which merges with previous detection results. This method effectively reduces the number of invalid region proposal, but it may also make the proposed regions excessively concentrated. Kang *et al.* developed tubelet proposal networks (TPN) to generate tubelets rather than bounding boxes. Then, an encoder-decoder LSTM is used for classification. TPN integrates temporal information, but it requires the future messages. Such methods are extended

from two-stage detectors, so they still suffer the problem with time efficiency.

2.3. Tracking and Detection

Object tracking is able to localize targets in a video with the prior knowledge of the initial position [24, 37, 38]. Ning *et al.* proposed ROLO based on YOLO and LSTM for tracking. YOLO is responsible for static detection, and the visual features and positions of high-score objects will be fed to LSTM for temporally modeling. Feichtenhofer *et al.* combined RFCN detector with correlation-filter-based tracker [37] to detect objects in a video, called D&T [23]. Thanks to tracking method, they achieve the high precision in terms of video detection, but obviously, the two-stage detector RFCN in D&T is not capable of temporal analysis. Moreover, the correlation filter could hardly work in real time, especially when a large number of objects appear in a video snippet.

2.4. RNN-Based Detector

Very recently, Up-to-date approaches have associated the detector with RNN. Liu and Zhu reported a mobile video detection method based on SSD and LSTM, called LSTM-SSD. Moreover, they also designed a Bottleneck-LSTM structure to reduce computational costs. As a result, LSTM-SSD reach a real-time inference speed of up to 15 FPS on a mobile CPU. Xiao and Lee developed a spatial-temporal memory module (STMM) with ConvGRU [15] for temporal information propagation [28]. In particular, “MatchTrans” was proposed to suppress the redundant memory.

3. Approach

In this section, we firstly present the proposed architecture, including HL-TU and AC-LSTM. We then describe in detail how to train the network.

3.1. Architecture

Extending from SSD with VGG-16 [26] as the base network, we build a temporal single-shot detector for robotic vision. Referring to the Fig. 2, the proposed TSSD is based on forward CNN that generate a fixed number of bounding boxes and the category-discriminative scores indicating the presence different classes of objects on those boxes, followed the non-maximum suppression (NMS) to generate the final results. The spatial resolution of input image is 300×300 , and the pyramidal features’ size are $38 \times 38 \times 512$, $19 \times 19 \times 512$, $10 \times 10 \times 512$, $5 \times 5 \times 256$, $3 \times 3 \times 256$, and $1 \times 1 \times 256$, respectively. As for sequence learning, the TSSD is equipped with the a multi-scale feature-integration structure, i.e. HL-TU and AC-LSTM. The HL-TU takes aim at propagation of pyramidal feature hierarchy in low computational costs, where as AC-LSTM aims

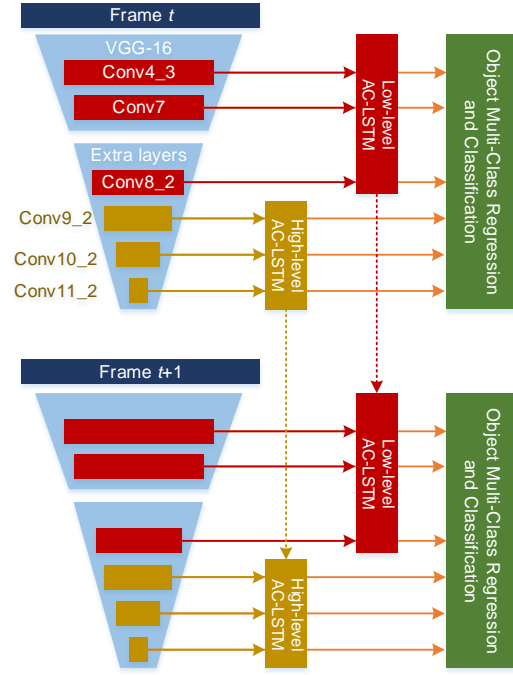


Figure 2. The proposed TSSD architecture. The high-level features share an AC-LSTM and low-level features do so, namely, HL-TU. Next, the hidden states of ConvLSTM will be used for multi-box regression and classification. Eventually, online tubelet analysis is conducted.

to effectively produce temporal memory without redundant features.

3.1.1 HL-TU

We use the same two structures to integrate the pyramidal feature hierarchy temporally, called HL-TU. There are pyramidal features for six-scale semantic information in adopted SSD model, and their receptive fields are diverse from each other. Creatively, we divide the multi-scale feature maps into two categories according to the size of receptive fields, i.e., high-level features and low-level features. Therefore, as shown in Fig. 2, we treat the first three feature maps as low-level features, whereas the last three maps are considered as high-level features. Their respective field sizes increase gradually for multi-scale objects. Correspondingly, the HL-TU including a high-level temporal unit and a low-level one are designed for them.

3.1.2 AC-LSTM

In object detection task, most features are related to background, and in addition, feature maps in different scales

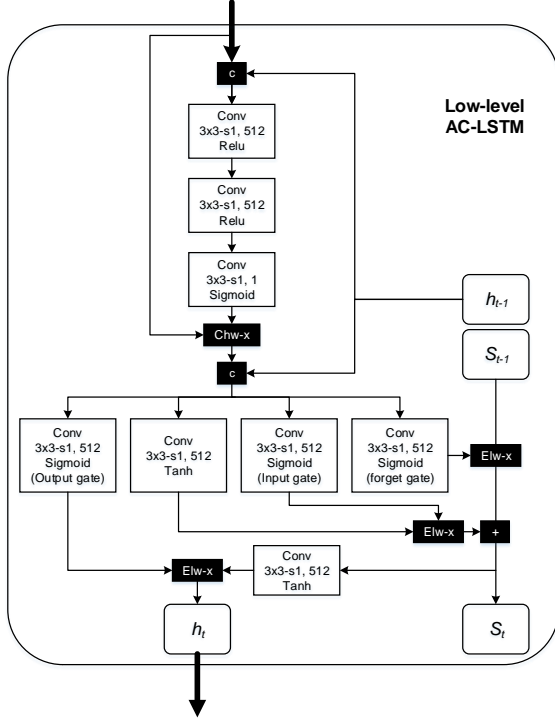


Figure 3. Implementation detail of AC-LSTM, including ConvLSTM-based attention and attention-based ConvLSTM. “c” denotes concatenation; “Chw-x”, “Elw-x” represent channel-wise and element-wise multiplication, respectively; “+” is element-wise summation.

contribute to detection in different degrees. Therefore, it is inefficient when a ConvLSTM handles background or aforementioned small-contributed multi-scale feature maps. For example, if an object’s size is too small, its detection will be contributed by the lowest-level feature map, in which features associated to the small object are far less than that for background. Moreover, all the higher-level feature maps can be considered useless, which should be suppressed to avoid the false positive. To that end, we propose AC-LSTM for background suppression and scale suppression, in which a temporal attention module selects object-related features for a ConvLSTM, and in turn, the ConvLSTM provides the attention module with temporal information to improve attention accuracy. As shown in Fig. 2, one of the low-level feature maps serves as the input of low-level AC-LSTM framework. Instead of computing attention map using the current feature, we firstly concatenate the input with previous information. Further, an attention map is generated, which suppresses redundant information. Thereby, the ConvLSTM integrates current attention-aware feature with previous information more effectively. Finally,

the current hidden state will be used for multi-box regression and classification. As a temporal analysis unit, AC-LSTM can be formulated as follows,

$$\begin{aligned}
 a_t &= \sigma(W_a * [x, h_{t-1}]) \\
 i_t &= \sigma(W_i * [a_t \odot x, h_{t-1}] + b_i) \\
 f_t &= \sigma(W_f * [a_t \odot x, h_{t-1}] + b_f) \\
 o_t &= \sigma(W_o * [a_t \odot x, h_{t-1}] + b_o) \\
 c_t &= \tanh(W_c * [a_t \odot x, h_{t-1}] + b_c) \\
 s_t &= (f_t \odot s_{t-1}) + (i_t \odot c_t) \\
 h_t &= o_t \odot \tanh(s_t)
 \end{aligned} \quad (1)$$

where $*$ denotes convolution operation; $[\cdot, \cdot]$ is concatenation; \odot is element-wise multiplication; and \circ represents that a one-channel map multiplies with each channel in a multi-channel feature map. At time step t , $a_t, h_t, i_t, f_t, o_t, c_t, s_t$ are attention map, hidden state, input gate, forget gate, output gate, new information in LSTM, and LSTM’s memory, respectively. σ represents sigmoid activation function.

As shown in Fig. 3, the AC-LSTM is designed with CNN and RNN. Current feature map (x) and previous hidden state (h_{t-1}) serve as the input of the attention module. After three-layer convolution, a one-channel attention map (a) is generated, which contains pixel-wise positions for object-related features. For feature selection, each channel of current feature map multiplies this attention map pixel-by-pixel, and the attention-aware feature ($a \odot x$) can be obtained. The attention-aware feature and previous hidden state are concatenated as the input of the ConvLSTM. Different from traditional LSTM, gates (i, f, o) and new information (c) will be computed with convolution operation [14]. Subsequently, controlled by the gates, the temporal memory (s) will be updated, and new hidden state is generated for multi-box regression and classification. During this operation, $a \odot x, i, f, o, c, s, h$ are in the same size.

Note that the attention module and input gate play different roles, although both of them can be aware of useful features. For background suppression and scale suppression, the attention module works for spatial location in each 2-D map, whereas the input gate can deal with the 3-D feature along the channel to preserve discriminative data.

3.2. Training

We design a multi-task objective to train TSSD, including a localization loss \mathcal{L}_{loc} , a confidence loss \mathcal{L}_{conf} , an attention loss \mathcal{L}_{att} , and an association loss \mathcal{L}_{asso} ,

$$\mathcal{L} = \frac{1}{M}(\alpha\mathcal{L}_{loc} + \beta\mathcal{L}_{conf}) + \gamma\mathcal{L}_{att} + \xi\mathcal{L}_{asso}, \quad (2)$$

where M is the number of matched boxes.

Subsequently, we train TSSD through three steps.

3.2.1 Localization Loss

At first, smooth-L1 loss is employed for regression [9]. In accordance with SSD, the regression is for the offset in terms of center (c_x, c_y), width (w), height (h) among the SSD's default boxes (d), predicted boxes (p), and ground truth boxes (g),

$$\begin{aligned}\mathcal{L}_{loc} &= \sum_{i=1}^N \sum_{n \in \{c_x, c_y, w, h\}} m_{i,j}^{cls} L(p_i^n - \hat{g}_j^n), \\ \hat{g}_j^{c_x} &= (g_j^{c_x} - d_i^{c_x})/d_i^w, \quad \hat{g}_j^{c_y} = (g_j^{c_y} - d_i^{c_y})/d_i^h, \\ \hat{g}_j^w &= \log(g_j^w/d_i^w), \quad \hat{g}_j^h = \log(g_j^h/d_i^h),\end{aligned}\quad (3)$$

where i is the subscript of N positive boxes, and $m_{i,j}^{cls} = 1$ if the i -th predicted box match j -th ground truth box in terms of category cls . Otherwise, $m_{i,j}^{cls} = 0$. L represents the smooth-L1 function.

3.2.2 Confidence Loss

After softmax operation, c_i^{cls} is used to represent the probability that the i -th predicted box belongs to class cls ($cls = 0$ for background). Thereby, the confidence loss is formulated as a cross entropy,

$$\mathcal{L}_{conf} = - \sum_{i=1}^N m_{i,j}^{cls} \log(c_i^{cls}) - \sum_{k=1}^{\delta N} \log(c_k^0), \quad (4)$$

where k is the subscript of δN negative boxes, and δ is the negative-to-positive ratio. Hard negative mining is employed to select negative boxes [9].

3.2.3 Attention Loss

We also supervise the generation of attention maps using cross entropy. At first, we construct the ground truth attention map A_g , in which elements in ground truth boxes equal to 1 and others are 0. There are six feature maps for multi-box prediction, which generate multi-scale attention maps $A_{p_{sc}}$. Therefore, $A_{p_{sc}}$ is firstly unified to the same resolution as the input image through bilinear upsampling operation, followed by the produce of $A_{p_s}^{up}$. Then, \mathcal{L}_{att} can be given as

$$\mathcal{L}_{att} = \sum_{sc=1}^6 \mu(-A_{p_{sc}}^{up} \log(A_g) - (1 - A_{p_{sc}}^{up}) \log(1 - A_g)), \quad (5)$$

where μ averages all elements of a matrix.

3.2.4 Association Loss

Towards temporal consistency of videos, an association loss is developed for sequence training. We firstly compute top k

high predicted scores per class after non-maximum suppression, and then sum them to generate a class-discriminative score list (sl). The score list should remain small fluctuation in consecutive frames. Thereby, the \mathcal{L}_{asso} can be obtained by,

$$\mathcal{L}_{asso} = \left(\sum_{t=1}^{seq_len} sl_t - sl_{ave} \right) / seq_len, \quad (6)$$

where sl_t is the score list at time step t ; sl_{ave} denotes the mean score list among $sl_{1:t-1}$; and seq_len represents the sequence length.

3.2.5 Multi-Step Training

At first, we train an SSD model following [9]. In the next step, TSSD is trained based on well-trained SSD. We freeze the weights in the network except for AC-LSTM and detection head (i.e., parameters for regression and classification). In particular, the ConvLSTM is trained with RMSProp [39] while the rest of TSSD is trained using SGD optimizer with the initial learning rate is 10^{-4} and a decay rate of 0.1 for 30 epochs. TSSD should be trained with a sequence of frames, but the frame rates of videos are inconstant. Moreover, the motion speed of objects in videos is of big difference. For better generalization, it should not be trained frame by frame. Instead, we only choose seq_len frames in a video for back propagation in an iteration. The seq_len frames should be chosen uniformly based on the start frame sf and skip sp ,

$$\begin{aligned}sp &= R[1, v/seq_len] \\ sf &= R[1, v - seq_len * sp + 1]\end{aligned}, \quad (7)$$

where v is the total number of frames in a video, and $R[min, max]$ represents the operation of selecting an integer randomly between min and max . Finally, the uniform seq_len frames are chosen with sf as the start frame and sp as the skip. In this paper, $seq_len = 8$. At this step, the association loss \mathcal{L}_{asso} is not involved.

Thirdly, the full objective including \mathcal{L}_{asso} is used to fine tune parameters for 10 epoches. At this step, the learning rate is 10^{-5} , and $sp = 1$. The hyper parameters $\alpha = 1, \beta = 1, \gamma = 0.5, \xi = 2, \delta = 3$ are selected based on the performance of validation set.

3.3. Inference

At inference phase, the base network and extra layers extract multi-scale features. Subsequently, HL-TU and AC-LSTM integrate those features through time, and then generate temporally-aware hidden state for regression and classification. Finally, we apply the non-maximum suppression with jaccard overlap of 0.45 per class and retain the top 200 high confident detections per image to produce the final detection results.

4. Experiment

4.1. Experiment Setup

4.1.1 Dataset

We evaluate TSSD on the ImageNet dataset for object detection from video (VID) [27], which is the biggest dataset for temporal object detection now. The task requires the algorithm detects 30-class targets in consecutive frames. There are 4000 videos in the training set, containing 1181113 frames. On the other hand, the validation set compasses 555 videos, including 176126 frames. We measure performance as mean average precision (mAP) over the 30 classes on the validation set following [4, 9].

In addition, ImageNet DET dataset is employed as training assistance. The 30 categories in VID dataset are a subset of the 200 categories in the DET dataset. Therefore, following [17, 18, 22, 23], we train TSSD with VID and DET (only using the data from the 30 VID classes).

In reality, There are millions of frames in VID training set, so it is hard to train a network directly using them. Additionally, the data for each category are imbalance, because there are long video (contains more than 1000 frames) and short video (contains only a dozen frames). Thus, following [23], we sample at most 2000 images per class from DET, and select 10 frames in each VID video for SSD training at the first step. In the second and third steps, all the VID training videos are adopted.

4.1.2 Running Environment

Our method is implemented under the PyTorch framework. The training and experiments are carried out on a workstation with an Intel 2.20 GHz Xeon(R) E5-2630 CPU, NVIDIA TITAN-X GPUs, 64 GB of RAM, CUDA 8.0, and cuDNN v6.

4.2. Ablation Study on ImageNet VID

Our methods progressively improves the object detection performance.

4.2.1 HL-TU

The HL-TU has addressed two problems. i) Redundant parameters are avoided. For example, the original SSD contains 2.6 M parameters, and SSD with HL-TU has 4.9 M parameters. However, if six ConvLSTMs are employed for each feature map, the amount of parameter will dramatically increase to 15.5M. ii) As reported in [25], the highest-level and lowest-level feature maps make relatively less contribution to detection. That is, there are a small amount of data for oversized or tiny-size objects. Thus, the highest-level and lowest-level ConvLSTMs can hardly be well trained, if six-scale ConvLSTMs are employed.

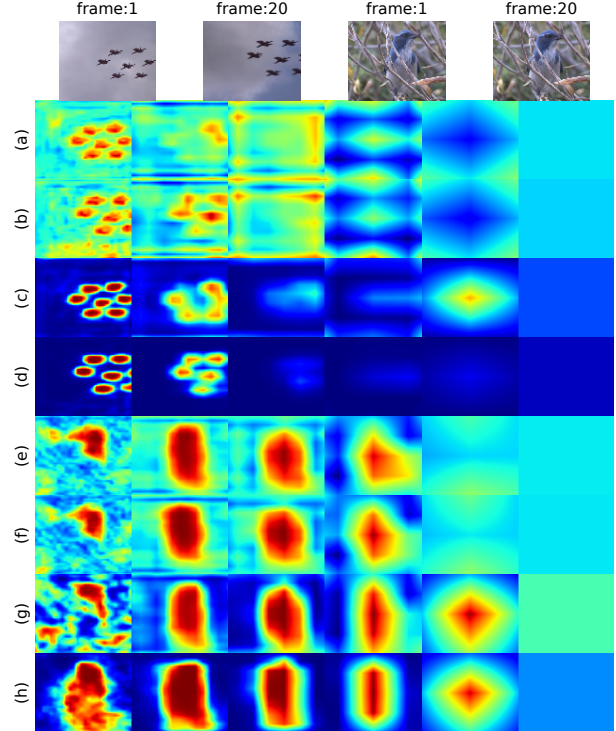


Figure 4. Effect of the ConvLSTM for attention module. There are two video snippets containing small objects (airplane) or wild environment (bird). The traditional attention and temporal attention module are used to generate multi-scale attention maps, in which darker red denotes higher level of concern while dark blue represents something neglected. (a)–(b) attention maps for airplanes generated by traditional module; (c)–(d) attention maps for airplanes generated by temporal module; (e)–(f) attention maps for bird generated by traditional module; (g)–(h) attention maps for bird generated by temporal attention module; In above 4 pairs maps, the former is for the first frame while the latter is with respect to the 20th frames. Each line in (a)–(h) is multi-scale attention maps, and higher-level maps are displayed on the righter.

We find that the mAP increase by 0.92% when HL-TU is adopted using two ConvLSTM as its temporal units due to the feature integration brought by ConvLSTMs.

4.2.2 AC-LSTM

At first, we analyze the interaction of attention module and ConvLSTM. As shown in Fig. 4, the comparison of temporal and traditional attention modules are presented. Note that the traditional attention module only uses current feature map as the input. In presented heat maps (i.e., Fig. 4 and Fig. 5), darker red means a higher probability of being a target, whereas the darker blue indicates ignorable pixel position in feature maps. Moreover, multi-scale attention maps are generated in TSSD, the righter maps response higher-level features. For the ease of observation, the multi-

Table 1. AP list on ImageNet VID validation set by the proposed.

Component	TSSD				
Association loss?	✓				
AC-LSTM?	✓	✓			
HL-TU?	✓	✓	✓		
Static-Attention?				✓	
mAP(%)	65.43	64.77	63.95	63.52	63.03

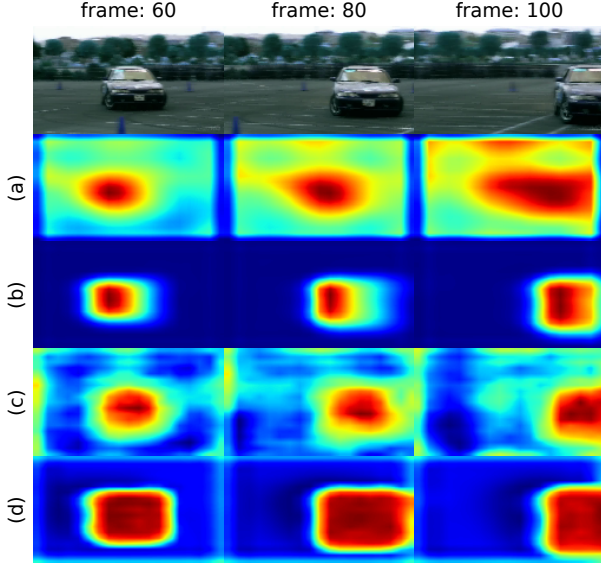


Figure 5. Effect of the temporal attention for ConvLSTM. The ConvLSTM’s memory (s) and hidden state (h) are visualized (by computing the L2 norm across feature channels at each spatial location to get a saliency map). (a) original ConvLSTM’s memories; (b) ConvLSTM’s memories in AC-LSTM; (c) original ConvLSTM’s hidden states; (d) ConvLSTM’s hidden states in AC-LSTM.

scale attention maps have been unified to the same spatial resolution as the input image through bilinear upsampling operation.

We choose two challenging scenes in this experiment. The airplane frames include small objects, and the bird frames contain rich stripes, both of which are difficult for attention operation. As shown in Fig. 4(a), (b), (e), (f), the original attention method is not able to handle these two scenes. That is, although the targets are focused roughly, the background and small-contributed multi-scale feature maps are not suppressed effectively. Moreover, there is no improvement through time steps. On the contrary, as illustrated in Fig. 4(c), (d), (g), (h), the proposed attention module performs better. The proposed attention method not only localizes the targets more accurately, but also suppresses the background more efficiently. Further, our method is effective for scale suppression. For instance, small objects in airplane frames are detected by the lowest-level feature map.

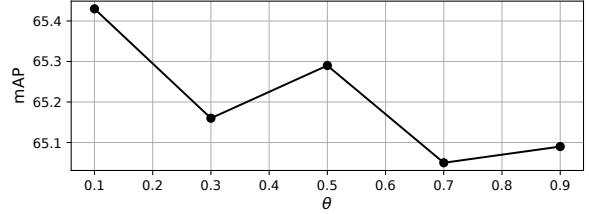


Figure 6. Model Performance vs. θ . This figure shows model performance as a function of the confidence threshold θ in association loss function.

As shown in Fig. 4(d), the first two attention maps localize airplanes, and all the last four maps are “cold”. That is, in terms of larger scale, our attention module can not find any target, so the whole of feature map has been suppressed. In addition, the performance of proposed approach improves along with the accumulation of temporal information. For example, in Fig. 4(g), (h), the lowest-level attention map can hardly find the bird in the first frame, but the bird’s body is focused without overmuch background in the 20th frame. Moreover, if attention maps for the first frame are compared, a conclusion can be drawn that the temporal attention module is better even though the temporal information has not generated. The reason is that it can be trained more effectively.

On the other hand, there are benefits of the AC-LSTM over traditional ConvLSTM. Referring to Fig. 5, the ConvLSTM’s memory and hidden state for the second-scale feature tensor are visualized. Compared with original ConvLSTM, the attention-based ConvLSTM produces more clear memories with pivotal features. Correspondingly, the hidden state of attention-based ConvLSTM is able to accurately cover the current object without complex background.

Due to the above reasons, the improvement bought by AC-LSTM is evident. That is, the mAP rise by 1.74% based on SSD.

4.2.3 Association Loss

In consideration of the employed NMS, there are three setting for computing association loss, i.e., confidence threshold θ , jaccard overlap threshold, and top k retained boxes.

Table 2. Comparison of TSSD and several prior and contemporary approaches.

Method	Components							Performances		
	1-stage	2-stage	BaseNet	OF	Track	Att	RNN	RT	Online	mAP
T-CNN [18]		✓	DeepID+Craft[32, 33]	✓	✓				✓	61.5
TPN [22]		✓	GoogLeNet[34]				✓			68.4
D&T [23]		✓	ResNet-101[35]		✓				✓	79.8
FGFA[30]		✓	ResNet-101	✓					✓	76.3
STSN [41]		✓	ResNet-101							78.7
Object-link[40]		✓	ResNet-101						✓	80.6
Closed-loop [20]		✓	VGG-M[31]						✓	50.0
STMN[28]		✓	VGG-16				✓			55.6
Seq-NMS [19]			VGG-16						✓	52.2
LSTM-SSD[29]	✓		MobileNet[36]				✓	✓	✓	54.4
TSSD(proposed)	✓		VGG-16			✓	✓	✓	✓	65.4

OF: Optical flow; Att: Attention.

Because of the NMS, the number of retained boxes is relatively insensitive, and the jaccard overlap threshold could be consistent with that in the inference phase. Thus, the major implication of \mathcal{L}_{asso} is θ , which indicates what kind of objects need to be involved. In this experiment, we set $k = 75$ to explore the impact of θ . As depicted in Fig. 6, the mAP generally decreases as θ increasing. Taking into account low score object or background, \mathcal{L}_{asso} is more effective when $\theta = 0.1$. Consequently, the TSSD achieve 65.43% as a mAP.

4.3. Comparison with Other Architectures

We also compare TSSD against several prior and contemporary approaches. As shown in Table 2, their components and performances have been summarized. Most methods are based on two-stage detector with RPN for region proposal. According to the authors' knowledge, TSSD is the first temporal one-stage detector achieving above 65% mAP with such small input images. In addition, few approaches successfully adopt attention or LSTM for temporal coherence, especially ConvLSTM. On the other hand, tracking employed in TCN [17], TCNN [18], and D&T [23] is a good idea for video detection, but each object needs a tracking filter. Thus, tracking affects time efficiency heavily, especially when target number increases. There should be two extra explanations for Table 2. i) The mAP for D&T, FGFA, Object-link, and STSN are quite high, and this performance is based on the employed two-stage detector with ResNet-101 as the base network. For example, the mAP for ResNet-based RFCN achieves 74.2% [23]. ii) TPN, STMN, and STSN use previous and further frames for current frame detection, so it is not an online detector. It is obvious that detector for robotic vision should be real-time and online, so TSSD is able to detect objects temporally for robots.

5. Conclusion

This paper has aimed at temporally detecting objects in real time for robotic vision. A creative TSSD approach is proposed. Differing from existing video detection methods, the TSSD is a temporal one-stage detector, and it can perform well in terms of both detection precision and inference speed. To efficiently integrate pyramidal feature hierarchy, HL-TU is proposed, in which the high-level features and low-level features share their respective temporal units. For background suppression and scale suppression, attention mechanism is employed to reduce information redundancy. Thereby, we design AC-LSTM as a temporal analysis unit, where the temporal attention module is responsible for selecting object-related features for the ConvLSTM. A novel association loss function is also designed for sequence training. As a result, the TSSD achieves considerably enhanced detection precision. Furthermore, owing to its real-time online characteristic, the TSSD is well-suited to robot's intelligent perception.

In the future, we plan to investigate the stability of temporal detection. In addition, the TSSD will be used for robotic visual navigation under dynamic environments.

References

- [1] A. Nguyen, D. Kanoulas, D. G. Caldwell, and N. G. Tsagarakis, "Object-based affordances detection with convolutional neural networks and dense conditional random fields," in *Proc. IEEE/RSJ Int. Conf. Intell. Robots and Syst.*, Vancouver, BC, Canada, Sep. 2017, pp. 24–28.
- [2] R. Girshick, J. Donahue, T. Darrell, and J. Malik, "Rich feature hierarchies for accurate object detection and semantic segmentation," in *Proc. IEEE*

- Conf. Comput. Vis. Pattern Recognition*, Columbus, the U.S., Jun. 2014, pp. 580–587.
- [3] R. Girshick. “Fast R-CNN,” in *Proc. IEEE Int. Conf. Comput. Vis.*, Santiago, Chile, Dec. 2015, pp. 1440–1448.
 - [4] S. Ren, K. He, R. Girshick, and J. Sun, “Faster R-CNN: Towards real-time object detection with region proposal networks,” in *Proc. Adv. in Neural Info. Proc. Syst.*, Montreal, Canada, Dec. 2015, pp. 91–99.
 - [5] K. He, G. Gkioxari, P. Dollar, and R. Girshick. “Mask R-CNN,” Venice, Italy, Oct. 2017, pp. 2961–2969.
 - [6] J. Dai, Y. Li, K. He, and J. Sun, “R-FCN: Object detection via region-based fully convolutional networks,” in *Proc. Adv. in Neural Info. Proc. Syst.*, Barcelona, Spain, Dec. 2016, pp. 379–387.
 - [7] T. Y. Lin, P. Dollar, R. Girshick, K. He, B. Hariharan, S. Belongie, “Feature pyramid networks for object detection,” in *arXiv:1612.03144*, 2016.
 - [8] J. Redmon, S. Divvala, R. Girshick, and A. Farhadi, “You only look once: Unified, real-time object detection,” in *Proc. IEEE Conf. Comput. Vis. Pattern Recognition*, Las Vegas, the U.S., Jun. 2016, pp. 779–788.
 - [9] W. Liu, D. Anguelov, D. Erhan, C. Szegedy, S. Reed, C. Y. Fu, and A. C. Berg, “SSD: Single shot multibox detector,” in *Proc. Eur. Conf. Comput. Vis.*, Amsterdam, Netherlands, Oct. 2016, pp. 21–37.
 - [10] T. Y. Lin, P. Goyal, R. Girshick, K. He, and P. Dollar, “Focal loss for dense object detection,” Venice, Italy, Oct. 2017, pp. 2980–2988.
 - [11] Y. Zhang, M. Pezeshki, P. Brakel, S. Zhang, C. L. Y. Bengio, and A. Courville, “Towards end-to-end speech recognition with deep convolutional neural networks,” *arXiv:1701.02720*, 2017.
 - [12] I. Sutskever, O. Vinyals, and Q. V. Le, “Sequence to sequence learning with neural networks,” in *Proc. Adv. in Neural Info. Proc. Syst.*, Montreal, Canada, Dec. 2014, pp. 3104–3112.
 - [13] S. Hochreiter and J. Schmidhuber, “Long short-term memory,” *Neural Comput.*, vol. 9, no. 8, pp. 1735–1780, 1997.
 - [14] X. Shi, Z. Chen, H. Wang, D. Yeung, W. Wong, W. Woo, “Convolutional LSTM network: A machine learning approach for precipitation nowcasting,” in *Proc. Adv. in Neural Info. Proc. Syst.*, Montreal, Canada, Dec. 2015, pp. 802–810.
 - [15] S. Valipour, M. Siam, M. Jagersand, and N. Ray, “Recurrent fully convolutional networks for video segmentation,” *arXiv:1606.00487*, 2016.
 - [16] V. Mnih, N. Heess, and A. Graves, “Recurrent models of visual attention,” in *Proc. Adv. in Neural Info. Proc. Syst.*, Montreal, Canada, Dec. 2014, pp. 2204–2212.
 - [17] K. Kang, W. Ouyang, H. Li, X. Wang, “Object detection from video tubelets with convolutional neural networks,” in *Proc. IEEE Conf. Comput. Vis. Pattern Recognition*, Las Vegas, the U.S., Jun. 2016, pp. 817–825.
 - [18] K. Kang, H. Li, J. Yan, X. Zeng, B. Yang, T. Xiao, C. Zhang, Z. Wang, R. Wang, X. Wang, and W. Ouyang, “T-CNN: Tubelets with convolutional neural networks for object detection from videos,” *IEEE Trans. Circuits Syst. Video Technol.*, DOI:10.1109/TCSVT.2017.2736553.
 - [19] W. Han, P. Khorrami, T. L. Paine, P. Ramachandran, M. Babaeizadeh, H. Shi, J. Li, S. Yan, and T. S. Huang, “Seq-NMS for video object detection,” *arXiv:1602.08465*, 2016.
 - [20] L. Galteri, L. Seidenari, M. Bertini, and A. Del Bimbo, “Spatio-temporal closed-loop object detection,” *IEEE Trans. Image Process.*, vol. 26, no. 3, pp. 1253–1263, 2017.
 - [21] S. Tripathi, S. Belongie, Y. Hwang, and T. Nguyen, “Detecting temporally consistent objects in videos through object class label propagation,” in *Proc. IEEE Winter Conf. Appl. Comput. Vis.*, New York, the U.S., Mar. 2016, pp. 1–9.
 - [22] K. Kang H. Li, T. Xiao, W. Ouyang, J. Yan, X. Liu, and X. Wang, “Object detection in videos with tubelet proposal networks,” in *Proc. IEEE Conf. Comput. Vis. Pattern Recognition*, Hawaii, the U.S., Jul. 2017, pp. 727–735.
 - [23] C. Feichtenhofer, A. Pinz, A. Zisserman, “Detect to track and track to detect,” in *Proc. IEEE Conf. Comput. Vis. and Pattern Recognition*, Venice, Italy, Oct. 2017, pp. 3038–3046.
 - [24] G. Ning, Z. Zhang, C. Huang, X. Ren, H. Wang, C. Cai, and Z. He, “Spatially supervised recurrent convolutional neural networks for visual object tracking,” in *Proc. IEEE Int. Symp. Circuits and Syst.*, Baltimore, the US, May. 2017, pp. 1–4.
 - [25] Y. Lu, C. Lu, and C. K. Tang, “Online video object detection using association LSTM,” in *Proc. IEEE Int. Conf. Comput. Vis.*, Venice, Italy, Oct. 2017, pp. 2344–2352.

- [26] K. Simonyan and A. Zisserman, “Very deep convolutional networks for large-scale image recognition,” *arXiv:1409.1556*, 2014.
- [27] O. Russakovsky, J. Deng, H. Su, J. Krause, S. Satheesh, S. Ma, Z. Huang, A. Karpathy, A. Khosla, M. Bernstein, A. C. Berg, and F. Li, “ImageNet large scale visual recognition challenge,” *Int. J. Comput. Vis.*, vol. 115, no. 3, pp. 211–252, 2015.
- [28] F. Xiao and Y. J. Lee, “Spatial-temporal memory networks for video object detection,” *arXiv:1712.06317*, 2017.
- [29] M. Liu and M. Zhu, “Mobile video object detection with temporally-aware feature maps,” *arXiv:1711.06368*, 2017.
- [30] X. Zhu, Y. Wang, J. Dai, L. Yuan, and Y. Wei, “Flow-guided feature aggregation for video object detection,” *arXiv:1703.10025*, 2017.
- [31] K. Chatfield, K. Simonyan, A. Vedaldi, and A. Zisserman, “Return of the devil in the details: Delving deep into convolutional nets,” in *Proc. Brit. Mach. Vis. Conf.*, Nottingham, the U.K., Sept., pp. 1-C12.
- [32] W. Ouyang, P. Luo, X. Zeng, S. Qiu, Y. Tian, H. Li, S. Yang, Z. Wang, Y. Xiong, C. Qian *et al.*, “Deepid-net: multi-stage and deformable deep convolutional neural networks for object detection,” *arXiv:1409.3505*, 2014.
- [33] B. Yang, J. Yan, Z. Lei, and S. Z. Li, “Craft objects from images,” in *Proc. IEEE Conf. Comput. Vis. and Pattern Recognition*, Las Vegas, the U.S., Jun. 2016, pp. 6043–6051.
- [34] C. Szegedy, W. Liu, Y. Jia, P. Sermanet, S. Reed, D. Anguelov, D. Erhan, V. Vanhoucke, and A. Rabinovich. “Going deeper with convolutions,” in *Proc. IEEE Conf. Comput. Vis. and Pattern Recognition*, Boston, the U.S., Jun. 2015, pp. 1–9.
- [35] Kaiming He, Xiangyu Zhang, Shaoqing Ren, Jian Sun, “Deep residual learning for image recognition,” *Proc. IEEE Conf. Comput. Vis. and Pattern Recognition*, Las Vegas, the U.S., Jun. 2016, pp. 770-778.
- [36] A. Howard, M. Zhu, B. Chen, D. Kalenichenko, W. Wang, T. Weyand, M. Andreetto, and H. Adam. “Mobilenets: efficient convolutional neural networks for mobile vision applications,” *arXiv:1704.04861*, 2017.
- [37] D. S. Bolme, J. R. Beveridge, B. A. Draper, and Y. M. Lui, “Visual object tracking using adaptive correlation filters,” in *Proc. IEEE Conf. Comput. Vis. Pattern Recognition*, San Francisco, the U.S., Jun. 2010, pp. 2544–2550.
- [38] D. Gordon, A. Farhadi, D. Fox, “Re3: Real-Time Recurrent Regression Networks for Visual Tracking of Generic Objects,” *arXiv:1705.06368*, 2017
- [39] T. Tieleman and G. Hinton, “Lecture 6.5-rmsprop: Divide the gradient by a running average of its recent magnitude,” *COURSERA: Neural Networks for Machine Learning*, vol.4, no. 2, pp. 26–31, 2012.
- [40] P. Tang, C. Wang, X. Wang, W. Liu, W. Zeng, and J. Wang, “Object detection in videos by short and long range object linking,” *arXiv:1801.09823*, 2018
- [41] G. Bertasius, L. Torresani, J. Shi, “Object detection in video with spatiotemporal sampling networks,” *arXiv:1803.05549*, 2018

Table 3. AP list on ImageNet VID validation set by the proposed method and compared methods.

Method	airplane	antelope	bear	bicycle	bird	bus	car	cattle	dog	d.cat	elephant
SSD	82.01	72.67	71.62	60.19	65.54	68.77	56.86	59.79	47.69	63.88	72.48
ConvLSTM	79.86	75.06	68.75	62.60	63.38	69.08	59.78	58.34	48.96	63.66	69.97
AC-LSTM	82.16	76.03	68.88	61.57	66.26	70.04	59.39	67.07	49.18	63.30	71.55
TSSD	81.53	76.55	68.32	64.04	66.29	68.89	60.18	65.11	49.83	64.88	71.72
Method	fox	g.panda	hamster	horse	lion	lizard	monkey	m.bike	rabbit	r.panda	sheep
SSD	77.47	79.04	89.04	61.53	26.43	61.34	41.78	73.58	49.20	20.96	58.99
ConvLSTM	80.61	78.03	90.12	62.53	28.17	62.15	41.25	75.69	54.33	44.90	56.19
AC-LSTM	80.85	80.71	90.18	63.36	30.21	64.61	41.50	75.81	56.00	39.85	57.24
TSSD	82.27	80.28	90.23	63.48	31.76	62.97	43.23	77.81	55.78	45.34	58.84
Method	snake	squirrel	tiger	train	turtle	w.craft	whale	zebra	FPS	mAP(%)	
SSD	47.95	47.11	80.71	76.98	69.07	61.61	63.54	83.34	~45	63.04	
ConvLSTM	46.41	45.95	81.18	76.03	70.33	62.56	58.65	83.96	~38	63.95	
AC-LSTM	49.34	46.14	82.45	77.68	71.49	62.02	54.58	83.23	~27	64.77	
TSSD	48.72	49.34	82.29	77.49	72.47	61.26	58.28	83.84	~27	65.43	

6. Complete Object Detection Results

We show the complete object detection results of the proposed TSSD method on the PASCAL ImageNet VID validation set in Table. 3. At first, SSD is employed as the baseline method. Then, we employ ConvLSTM following HL-TU and denote the result as “ConvLSTM”. Subsequently, AC-LSTM is adopted, followed by the result being called “AC-LSTM”. Finally, the result of proposed TSSD including HL-TU, AC-LSTM, and association loss are presented.

7. Qualitative Results

We show some qualitative results on the ImageNet VID validation set, in Figure 7. We only display the detected bounding boxes with the score larger than 0.5. Different colors of the bounding boxes indicate different object classes. The proposed TSSD works well with precision and temporal stability.

